6-1-2021

N-cadherin in osteolineage cells modulates stromal support of tumor growth

Francesca Fontana

Jingyu Xiang

Xinming Su

Eric Tycksen

Rachel Nassau

See next page for additional authors

Authors

Francesca Fontana, Jingyu Xiang, Xinming Su, Eric Tycksen, Rachel Nassau, Gregory Fox, Giulia Leanza, Katherine Weilbaecher, and Roberto Civitelli

Journal of Bone Oncology 28 (2021) 100356

Contents lists available at ScienceDirect

Journal of Bone Oncology

journal homepage: www.elsevier.com/locate/jbo

N-cadherin in osteolineage cells modulates stromal support of tumor growth

Francesca Fontana [a,b], Jingyu Xiang [b], Xinming Su [b], Eric Tycksen [c], Rachel Nassau [a], Gregory Fox [b], Giulia Leanza [a], Katherine Weilbaecher [b], Roberto Civitelli [a,*]

[a] Division of Bone and Mineral Diseases, Musculoskeletal Research Center, United States
[b] Division of Molecular Oncology, Department of Medicine, United States
[c] Genome Technology Access Center, Washington University School of Medicine, St. Louis, MO, United States

ARTICLE INFO

Article history:
Received 5 November 2020
Revised 3 February 2021
Accepted 9 February 2021
Available online 23 March 2021

Keywords:
N-cadherin
Bone-tumor cell interactions
Tumor microenvironment
Transcriptomics

ABSTRACT

Tumor growth and metastases are dependent on interactions between cancer cells and the local environment. Expression of the cell–cell adhesion molecule N-cadherin (Ncad) is associated with highly aggressive cancers, and its expression by osteogenic cells has been proposed to provide a molecular "dock" for disseminated tumor cells to establish in pre-metastatic niches within the bone. To test this biologic model, we conditionally deleted the Ncad gene (*Cdh2*) in osteolineage cells using *Osx-cre* (cKO). Contrary to expectations, the metastatic breast cancer cell line PyMT-BO1 was able to form tumors in bone and to induce osteolysis in cKO as well as in control mice. Despite absence of Ncad, bone marrow stromal cells isolated from cKO mice were able to engage in direct cell–cell interactions with tumor cells expressing either N- or E-cadherin. However, subcutaneous PyMT-BO1 and B16F10 tumors grew larger in cKO relative to control littermates. Cell tracking experiments using the Ai9 reporter revealed the presence of Osx+ and Ncad+ cells in the stroma of extra-skeletal tumors and in a small population of lung cells. Gene expression analysis by RNAseq of Osx+ cells isolated from extra-skeletal tumors revealed alterations of pro-tumorigenic signaling pathways in cKO cells relative to control Osx+ cells. Thus, Ncad in Osx+ cells is not necessary for the establishment of bone metastases, but in extra-skeletal tumors it regulates pro-tumorigenic support by the microenvironment.

1. Introduction

Metastases are responsible for 90% of cancer-related deaths, but each of the steps leading to their development entails a combination of events, both for "seed" cells to arise and reach the metastatic site and for "soil" environments to become receptive to tumor engraftment and growth of metastatic foci. Select tumor cells need to leave their site of origin, circulate, evade immune surveillance, adhere to a new "niche", and modify a new environment so as to allow their growth [1]. Cell-adhesion molecules have long been known to play a key role in tumor progression and metastases, as they represent a molecular mechanism for cells to orient in their surroundings and communicate with neighboring cells [2].

Among cell–cell adhesion molecules, cadherins are calcium-dependent *trans*-membrane glycoproteins that organize into adherens junctions, which provide cell–cell anchorage via linkage to the cytoskeleton [3]. Our group and others have shown that N-cadherin (Ncad) is the main cadherin expressed in bone cells, and that disruption of cadherin function or loss of the Ncad gene (*Cdh2*) in osteolineage cells leads to delayed skeletal growth, low bone mass and reduced osteoprogenitor number [4–6]. While Ncad is important for mesenchymal cell fate determination [6], our previous work has also shown that Ncad is dispensable for osteoblast support of the hematopoietic stem cell niche [7,8]. Aside from cell-cell adhesion, cadherins also modulate cell migration and specific signaling pathways. In particular, *Cdh2* deletion or haploinsufficiency negatively affects MAPK/p38 [9,10], ERK, PI3K/Akt [11] PTHR1 [12], and Wnt [5,13] pathways, whereas Ncad augments FGFR signaling [14,15]. Many of these signaling systems are involved in tumor growth.

During tumor development, some carcinoma cells undergo a "cadherin switch" from E-cadherin (Ecad) to Ncad, a hallmark of epithelial-to-mesenchymal transition [16,17]. There is ample in vitro and pre-clinical evidence suggesting that Ncad can favor tumor progression. Overexpression of Ncad in tumor cells

* Corresponding author at: Division of Bone and Mineral Diseases, Washington University in St. Louis, 660 South Euclid – Campus Box 8301, St. Louis, MO 63110, United States.
E-mail address: civitellir@wustl.edu (R. Civitelli).

https://doi.org/10.1016/j.jbo.2021.100356
2212-1374/

increases tumor cell migration and metastasis [18], while antibody neutralization of Ncad hinders migration of cancer cell lines in vitro and reduces metastases in xenograft models [19]. Further, N-cad inhibitors reduce the growth of Ncad overexpressing pancreatic tumors [20] and improve response to chemotherapy in preclinical models [21]. However, other preclinical studies show that Ncad functions as a growth suppressor in K-ras-induced murine pancreatic tumors [22], and interfering with Ncad may even stimulate tumor growth in some mouse models of melanoma [23]. More to the point, published clinical trials using Ncad antagonists for potential anti-tumorigenic action have been quite inconsistent [24,25], highlighting the need of a better understanding of the role of Ncad in tumorigenesis and cancer progression.

So far, research in this area has focused on Ncad in cancer cells, and less attention has been given to how cadherins in resident cells within the microenvironment contribute to the interaction between the tumor and the tissue in which it grows. Recent work has proposed that homo- or heterotypic interactions between Ncad or Ecad on cancer cells and Ncad on osteogenic cells mediate the engraftment of cancer cells in the bone marrow and eventually lead to the development of bone metastases, via interference with mTOR signaling [26]. Although these data support a pro-tumorigenic action of Ncad in bone metastasis, whether removal of Ncad from bone cells prevents bone metastasis, as predicted by this biologic model, or whether adhesion between bone and tumor cells is altered in the absence of Ncad, have not been tested experimentally.

In this work, we have used mice with conditional *Cdh2* ablation in osteolineage cells driven by the Osterix (Osx) promoter, which we have previously characterized [5,12], to ask whether lack of Ncad in osteogenic cells protects these mice from bone engraftment of cancer cells. Contrary to such expectations [26], we find that tumor cells, similarly to hematopoietic stem cells, do not require Ncad to engage in cell–cell adhesion with osteolineage cells. We also find that subcutaneous tumors contain a Ncad+ Osx+ stromal sub-population, which, upon loss of Ncad, causes tumors to grow faster and lung metastases to develop earlier. Our studies unveil an unexpected tumor-suppressive effect of Ncad in stromal cells of the tumor microenvironment.

2. Material and methods

2.1. Animal models

All animal studies were designed and performed according to the Animal Research Reporting of In Vivo Experiment (ARRIVE) guidelines [27]; animal protocols and procedures were approved by the Institutional Animal Care and Use Committee at Washington University in St. Louis (protocols 20140142 and 20170095). We used mouse models that we have previously described and characterized [5,7,12]. To mark osteolineage cells in vivo, we used either B6.Cg-Tg(Sp7-tTA,tetO-EGFP/cre)1Amc/J (Jackson laboratories) mice, which carry a tetracycline-responsive *Osx* promoter (*Osx*-Cre), or B6.Cg-Gt(ROSA)26Sor Tm9(CAG-tdTomato)Hze/J (Ai9) (Jackson Laboratories) mice, and mated then with $Cdh2^{Flx/Flx}$, to generate $Cdh2^{Flx/Flx}$::*Osx*-Cre mice (cKO), Ai9;$Cdh2^{Flx/Flx}$::*Osx*-Cre (Ai9-cKO) or Ai9:*Osx*-Cre. Unless otherwise indicated, all mice were 6–12-week-old at the time of cancer cell inoculation. Mice were housed in cages containing 2–5 animals each, in a room maintained at constant 25 °C on a 12-hour light/dark cycle, and fed an ad libitum regular chow (PicoLab Rodent Diet 20, 5053; TestDiet/LabDiet, St. Louis, MO), unless otherwise specified. We have shown that Osx-driven *Cdh2* cKO mice have stunted growth and low bone mass [5]. To exclude any confounding effect on tumor growth, in some experiments we delayed Osx-Cre activation and *Cdh2* ablation by suppressing the Tet-senstive Osx-Cre transgene with doxycycline (Doxy) until 4 weeks of age [5,28]. In such experiments, chow containing 200 ppm Doxy (Modified LabDiet 5058, 5BFB) was administered to dams and litters until weaning (age 24–28 days). Mice were euthanized by ketamine/xylazine (average of 150/15 mg/kg body weight) cocktail intraperitoneal overdose and terminal intracardiac bleeding as approved by Animal Studies Committee.

2.2. Cell lines and cultures

The B16-F10-Luc (B16) murine melanoma cell line (ATCC) is derived from B16-F10 cells modified to express firefly luciferase [29]. The 4T1-GFP-Luc (4T1) murine mammary tumor cell line, which stably expresses firefly luciferase (Luc) and green fluorescent protein (GFP) reporters, was generously provided by Dr. David Piwinica-Worms (MD Anderson Cancer Center, Houston, TX) and cultured as previously described [30]. The PyMT-BO1-GFP-Luc (BO1) cell line was derived from a primary tumor in MMTV-PyMT mice, and modified to stably express GFP and firefly Luc reporters [31]. The PyMT-B6 (B6) murine mammary tumor cell line, also derived from a MMTV-PyMT tumor, was kindly provided by Dr. David DeNardo (Washington University), and carries a click beetle red luciferase-mCherry reporter [32]. Bone marrow stromal cells (BMSC) were isolated from $Cdh2^{flx/flx}$ or *Cdh2*-cKO littermates by flushing of the bone marrow by centrifugation, and filtering over 70 μm cell strainers (VWR, Radnor, PA). They were cultured in ascorbic acid-free αMEM (Gibco) supplemented with 40 mM L-glutamine, 100 U/ml penicillin-G, 2.5 μg/mL amphotericin B, 100 mg/ml streptomycin, and 15% FBS. Cell cultures were kept at 37 °C in a humidified atmosphere with 5% CO_2; culture medium was replaced every 3–5 days, according to established methods [5,33]. Likewise, the mouse stromal cell line, ST2 [34], was cultured and maintained in αMEM with antibiotics, as just noted.

2.3. Mouse tumor models

For intratibial injection, 5×10^4 PyMT-BO1-GFP-Luc cells in PBS were injected in the left tibia under anesthesia with Ketamine/Xylazine cocktail (100/10 mg/Kg BW) using a procedure previously described [35], while PBS was injected in the right tibia. For mammary fat pad (MFP) injection, 1×10^5 PyMT-B6 (B6) expressing Luciferase and mCherry were mixed with matrigel (BD) and injected into the mammary tissue of 8-week-old female mice. To minimize differences between male and female subjects on tumor growth experiments, 5×10^5 BO1 cells mixed with matrigel were inoculated in the subcutaneous tissue of the flank of the mice. Gender stratification of experimental groups is reported in Table 1 and statistical analysis for gender effect on tumor growth showed no differences for the subcutaneous inoculation. For subcutaneous injections of melanoma cells, 1×10^6 B16 cells suspended in 100 μL PBS were injected into the flank, and tumor growth was measured at each indicated time point by caliper. Tumor size (mm^3) was calculated by measuring the longest (L) and shortest (S) diameters of tumor tissue using the formula: $0.5*L*S^2$.

2.4. Bioluminescence imaging

For live bioluminescence imaging (BLI), mice were shaved, injected intraperitoneally with 150 μg/g D-luciferin (Biosynth, Naperville, IL) in PBS, anesthetized with isoflurane 2.5%, and imaged with a charge-coupled device camera-based bioluminescence imaging system (IVIS 100; Caliper, Hopkinton, MA; exposure time 1–300 s, binning 8, field of view 12, f/stop 1, open filter, anterior side), following described procedures [36]. Signal was displayed as photons/sec, and regions of interest were defined

manually around the legs using Living Image and IgorPro Software by an examiner blinded to mice genotype (Version 2.50).

2.5. Ex-vivo radiography

For assessment of osteolytic lesions, legs were dissected by removing all skin and muscle tissues (but no extra-osseous tumor outgrowth), fixed in formalin 10% for 48 h and preserved in 70% ethanol until analysis. Digital contact radiographs were then taken using a Faxitron UltraFocus100 scanner (Faxitron Bioptics, Tucson, AZ, USA) and regions affected by osteolysis were measured using ImageJ software (National Institutes of Health, USA), as described [36], by an examiner blinded to genotype.

2.6. Flow cytometry of tissue homogenates

To determine the presence of tumor cells in the circulation, blood samples were obtained by cardiac puncture and collected in EDTA-coated microtitainers (BD). Mice were then perfused with PBS through left and right ventricle infusion and bones, lungs, and tumor tissues were resected. Bone marrow samples were obtained by centrifugation and resuspended in PBS 1% FBS. To obtain cell suspensions, tumors and lungs were minced and digested in 2 mg/ml collagenase A (Roche, Indianapolis, IN, USA) and DNAse in DMEM (MilliporeSigma, St. Louis, MO, USA) for 30 min at 37 °C. Digestions were quenched by washing with excess culture media (20% FBS) and cells filtered through 70 μm cell strainers (VWR). Red cell lysis was performed by incubating 10 min with red blood cell lysis solution (MilliporeSigma) and washed with excess PBS 1% FBS. For Ncad staining, samples were blocked with rat anti-mouse CD16/32 (Cat. 93, Biolegend, San Diego, CA, USA) for 10 min at room temperature, resuspended in 100 μL buffer with primary anti-Ncad antibody (Cat. 806–820, MilliporeSigma) and incubated on ice for 30 min, washed and incubated with APC-conjugated rabbit-anti-mouse on ice for 30 min. Propidium Iodide (20μg/sample) (MilliporeSigma) was used to stain for viability. Flow cytometry was performed with a BD FACSCalibur™ (BD) flow cytometer and analyzed by FlowJo (TreeStar/FlowJo LLC, Ashland, OR, USA).

2.7. Cell-Cell adhesion

To test gap junction intercellular communication (GJIC), we used a modification of a previously described method [37]. Tumor cells were trypsinized (0.25% Trypsin-EDTA, MilliporeSigma), resuspended in culture media, and loaded by 30-minute incubation in calcein-AM (Life Technology, Green Island, NY), when used as "donor" cells, or labeled with the membrane permanent dye, DiI (CellTracker™ CM-DiI, Thermo-Fisher Scientific, St. Louis, MO), when used as "acceptor" cells. Using the same procedures, BMSC were loaded with calcein-AM, and ST2 cells with DiI. To assess GJIC, DiI-labeled acceptor cells were "parachuted" onto a monolayer of calcein-loaded donor cells. After 2-h incubation to allow cell–cell adhesion and gap junction formation, the percentage of acceptor cells that had taken calcein from donor cells was determined by FACS as index of GJIC. As a negative control, sets of donor and acceptor cells were placed on either side of a transwell system (Corning, Lowell, MA), where they shared the culture medium but were physically separated by a 0.4 μm transwell. Optical microscopy images of tumor cells parachuted onto BMSC were obtained on an Axiovert S100 fluorescence microscope (Zeiss, Jena, Germany) at 40X magnification. Phase contrast and green and red fluorescence were then merged in ImageJ software (National Institutes of Health, USA). After 8 h incubation, cells were trypsinized, centrifuged and resuspended in FACS buffer for flow cytometry for quantification of red and green fluorescence. Data were acquired with a FACSCalibur™ (Becton, Dickinson and Company, Franklin Lakes, NJ, USA) flow cytometer, and analyzed by FlowJo 10.0.7 software (TreeStar/FlowJo LLC, Ashland, OR, USA). The percentage of doubly fluorescent cells (acceptor cells that have taken calcein) relative to the total red (acceptor) cells, was used as an index of GJIC.

To test adhesion-dependent resistance to the chemotherapeutic agent eirubulin [38], 4T1 cells were co-cultured with ST2 cells, exposed to 200 nM eribulin for 24 h, and released from the tissue culture dish by trypsin-EDTA for 5 min. As tumor cells detach more easily from plates and from each other than stromal cells, this procedure enriches the cell suspension for tumor cells, while stromal cells remain attached to the plate. Suspended cells were washed in cold PBS and prepared for cell cycle analysis as per Abcam protocol (https://www.abcam.com/protocols/flow-cytometric-analysis-of-cell-cycle-with-propidium-iodide-dna-staining). Briefly, cells were dehydrated in 70% ethanol for a minimum of 5 h at 4 °C, washed in ice-cold PBS, incubated with 5 μg RNAse A for 1 h at 37 °C, and stained with 20 ng Propidium Iodide (MilliporeSigma, St Louis, MO). After washing in PBS, pellets were resuspended in FACS buffer (PBS 2% FBS) and cells subjected to flow cytometry (BD FACSCalibur™, BD, Franklin Lake, NJ). FlowJo was used to identify peaks for G1, S, and G2 phases.

2.8. RNAseq analysis

To prepare cells for RNAseq analysis, subcutaneous tumors originating from injection of MMTV-BO1 cells in *Cdh2*-cKO;Ai9 and *Osx*-cre;Ai9 mice were excised and incubated with collagenase. Cells in suspension were stained for CD45 and sorted with a FACS Aria (BD) to exclude GFP + cells (tumor cells) and separate single positive CD45+, single positive Osx+ (tdTomato fluorescence) cells, and GFP- CD45−;Osx− triple-negative cells. To obtain adequate numbers of cells for transcriptomic analysis, we inoculated 6 *Cdh2*-cKO;Ai9 and 4 *Osx*-cre;Ai9 mice and selected, from these cell preparations, those samples that met the quality control test for RNA integrity (average RIN = 8.95). Based on this protocol, we submitted 2–3 biological replicates per group of cells, per each genotype to RNAseq analysis. Samples were prepared with the Clonetech SMARTer version 1 kit according to manufacturer's protocol, indexed, pooled, and sequenced across two 50 base-pair single-end Illumina HiSeq 3000 lanes on a single flowcell. Basecalls and demultiplexing were performed with Illumina's bcl2fastq software with a maximum of one mismatch in the indexing read. RNA-seq reads were then aligned to the Mus musculus Ensembl release 76 top-level assembly with STAR version 2.0.4b. Gene counts were derived from the number of uniquely aligned unambiguous reads by Subread:featureCount version 1.4.5. Sequencing performance was assessed for the total number of aligned reads, total number of uniquely aligned reads, and features detected. The ribosomal fraction, known junction saturation, and read distribution over known gene models were quantified with RSeQC version 2.3.

All gene counts were then imported into the R/Bioconductor package EdgeR and TMM normalization size factors were calculated to adjust for samples for differences in library size. Ribosomal genes and genes not expressed in at least two samples greater than one count-per-million were excluded from further analysis. The TMM size factors and the matrix of counts were then imported into the R/Bioconductor package Limma. Performance of the samples was assessed with principle components analysis. Weighted likelihoods based on the observed mean–variance relationship of every gene and sample were then calculated for all samples with the voomWithQualityWeights. Differential expression analysis was then performed to analyze for differences between the cKO Osx + CD45 negative cells and wild-type Osx + CD45 negative cells as well as the cKO double negative and wild-type double negative

cells. The results were filtered for only those genes with p-values less than or equal to 0.05 and log_2 fold -changes greater than an absolute value of 2.

For each contrast extracted with Limma, global perturbations in known Gene Ontology (GO) terms, MSigDb terms, and KEGG pathways were detected using the R/Bioconductor package GAGE to test for changes in expression of the reported log_2 fold-changes reported by Limma in each term versus the background log_2 fold-changes of all genes found outside the respective term. The R/Bioconductor package heatmap3 and Pathview were used to display heatmaps or annotated KEGG graphs across groups of samples for each GO term or KEGG pathway (respectively) with a Benjamini-Hochberg false-discovery rate adjusted p-value less than or equal to 0.05.

2.9. Statistical analysis

Statistical analyses were performed using Prism version 8 (GraphPad Software, Inc., La Jolla, CA, USA). Two-group comparisons were performed by Student's *t*-test. Multiple-group means were analyzed by one-away analysis of variance (ANOVA) followed by post hoc analysis for multiple group comparisons. Two-way ANOVA was used to analyze the contribution of multiple independent variables, and for repeated measures datasets. After ANOVA, Bonferroni or Sidak post-hoc test was used for comparison of individual data points. Mann-Whitney test was used for non-normally distributed data. Categorical data sets were compared using Fisher's exact test. Unless otherwise specified, data are expressed as median and interquartile range.

2.10. Data statement

Sequencing data are deposited in GEO under accession code GSE143586 https://www.ncbi.nlm.nih.gov/geo/query/acc.cgi?acc = GSE143586. All other research data are available upon request.

3. Results

3.1. Loss of Ncad in osteogenic cells does not affect cancer growth in bone, but favors tumor growth at extra-skeletal sites

As noted, Ncad in osteolineage cells has been proposed to mediate heterotypic interactions with Ecad in cancer cells and allow tumor cell homing to bone [26]. To test this biologic model, we inoculated BO1 cells, which have high propensity to metastasize to bone, into one tibia of cKO or *Cdh2*$^{flx/flx}$ littermates (henceforth noted as wild type-equivalent: WTe); PBS was injected in the contralateral tibia as control. To control for tumor growth at other sites, we also inoculated the B6 parental breast cancer cells (B6) into the mammary fat pad (MFP) of control and mutant mice. We first verified that while BO1 cells express *Cdh2* mRNA, B6 cells express Ecad more abundantly than Ncad (Sup. Fig. 1A, B). We noted no differences in tumor growth in tibiae of cKO mice relative to WTe by BLI followed for 2 weeks after tumor cell inoculation at 8 weeks of age (Fig. 1A left hindlimb circles, B). Closely similar results were obtained upon injection of BO1 cells in tibiae of Doxy treated mice, in which OsxCre is activated post-natally [28], with equal intratibial growth of BO1 tumors (Sup. Fig. 1C). On plain radiographs extensive bone destruction occurred equally in both genotypes in the inoculated tibia and in the adjacent femur (Fig. 1C), and there were no differences in tumor outgrowth through the cortex into the adjacent soft tissue area (Sup. Fig. 1D, E); whereas the contralateral, PBS-injected hind limbs, showed no overt signs of osteolysis (not shown). Surprisingly, BLI revealed not only larger orthotopic MFP tumors in cKO mice (Fig. 1A, squares) but also the presence of soft tissue activity in the chest of cKO mice, rapidly increasing with time (Fig. 1D). On necropsy, we found a larger number of lung metastases in cKO mice than in WTe control mice (Fig. 1E). Indeed, 70% of cKO developed metastases by day 10, vs. 40% of controls (5/7 vs 2/5) ($p < 0.05$, Fisher's test).

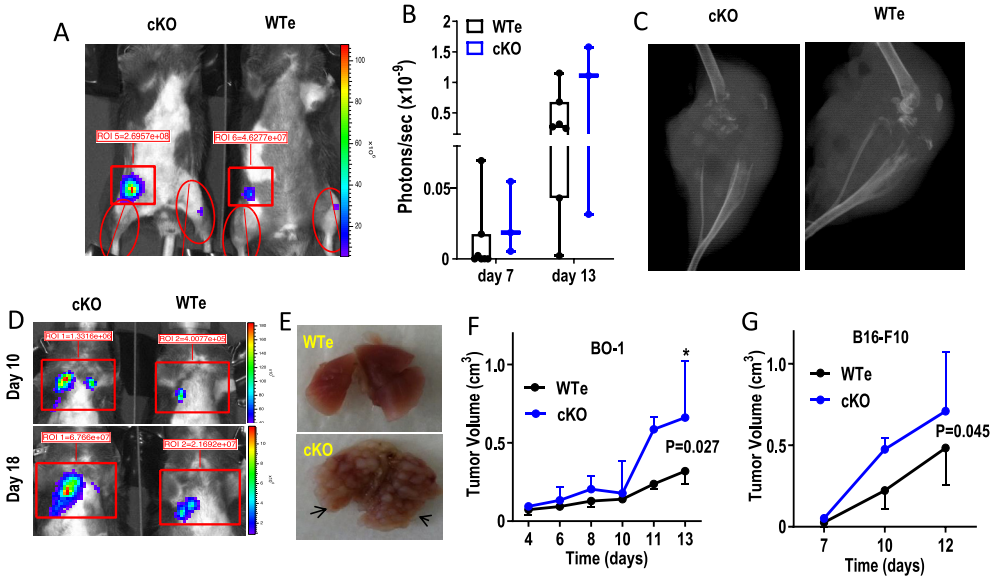

Fig. 1. Tumor growth in bone and extraskeletal tissues. Wild type equivalent (WTe) and cKO mice were inoculated with GFP-Luciferase-labeled BO1 cells in the left tibiae, and mCherry-Luciferase-labeled PyMT-B6 in the MFP. (A) Representative experiment showing engraftment in the tibia (right oval) and MFP (rectangle) in both mice by BLI. (B) Quantitation of BLI intensity at days 7 and 13 after tumor inoculation. (C) Plane radiographs of hindlimbs of WTe and cKO (treated with doxycycline during breeding) littermates 3 weeks after BO1 inoculation into the tibia showing extensive bone destruction. (D) Soft tissue chest BLI activity at day 10 and 18 after in WTe and cKO mice. (E) Presence of large and numerous metastatic nodules in the lungs of cKO relative to WTe mice inoculated with BO1 and B6 cells. Tumor growth, measured by caliper, over time after subcutaneous inoculation of either (F) B01 cells, or (G) B16 melanoma in WTe or cKO littermates (median and interquartile range; n = 3–6 per group). P-values reflect the genotype effect in a two-way ANOVA (for BO-1: genotype F = 10.43, p = 0.027; time F = 11.39, p < 0.001; interaction F = 1.85, p = 0.128. For B16-F10: genotype F = 4.60, p = 0.045; time F = 20.63, p < 0.001; interaction F = 0.94, p = 0.407). *p = 0.0015 vs. WTe, after Sidak's adjustment for multiple comparisons.

Therefore, we asked whether loss of Ncad in Osx+ cells might affect the growth of tumors outside the bone. To this end, we inoculated BO1 cells in the subcutaneous tissue of cKO and control littermates and followed tumor growth by caliper measurements. Tumor volume grew significantly larger with time in cKO mice compared to WTe littermates (Fig. 1F). The same result was consistently obtained in 4 independent experiments, regardless of doxycycline administration, with an overall increase of 30% in cKO vs WTe after 10–15 days post-inoculation (Table 1). Likewise, a significantly larger increase in tumor growth in cKO relative to WTe mice also occurred when the B16-F10 melanoma cell line was injected subcutaneously (Fig. 1G). Suggesting a possible increased lethality, 2/5 cKO mice died before two weeks after inoculation, while none died in the WTe group ($p = 0.07$; Fisher's test). Therefore, Ncad expression in osteogenic (Osx+) cells is not required for tumor growth in the bone and for tumor associated bone loss; however, loss of Ncad in osteogenic lineage, Osx+, cells alters the tumor microenvironment outside the bone, favoring tumor growth.

3.2. Loss of Ncad in osteogenic cells does not decrease dissemination of tumor cells to bone

To evaluate whether ablation of Ncad in these Osx+ osteogenic cells prevents bone metastasis, as it would be predicted if Ncad/Ecad interactions were required for early stages of metastases [26], we inoculated again the highly metastatic BO1 cells in the flank subcutaneous tissue of WTe and cKO mice, and let tumors grow until 2 cm of maximum diameter, before collection for flow cytometry (Fig. 2A). There was no difference in the number of bone marrow GFP+ cells – representing disseminated tumor cells (DTC) – between tumor-bearing WTe and cKO littermates (Fig. 2B). Likewise, we found no difference in the number of Ncad-expressing primary tumor cells (Sup. Fig. 2A); and cell viability within tumors was also similar between genotypes (Sup. Fig. 2B), suggesting that lack of Ncad in Osx+ cells does not prevent subcutaneous tumor cells from reaching and/or being retained in the bone. We then tested whether lack of Ncad in osteogenic cells may prevent tumor cell dissemination or permanence in the bone marrow and metastasis over the long-term. After subcutaneous inoculation of BO1 cells, we performed survival surgery (marginal resection) when tumors reached 1 cm diameter; then followed the mice for development of recurrence or metastases by BLI and survival until 175 days after inoculation (160–155 after surgery) (Fig. 2C). Tumor weight was well matched between genotypes at resection, confirming a balanced tumor burden (not shown). No mice developed local recurrence, but BLI showed signs of distant site metastases as soon as day 25 in 33% (2/6) of cKO and 11% (1/9) of WTe mice (Fig. 2D). Only one WTe mouse developed bone metastases; none were observed in cKO, and most metastatic foci were found in the lungs after 160–155 days from primary tumor resection. In most cases, there was more severe metastatic disease in cKO littermates, as exemplified in Sup. Fig. 2C. However, even though the median relapse-free survival (defined as evidence of recurrence by BLI or death) was reduced in cKO relative to WTe mice (41.5 vs. 89.0 days), the difference was not statistically significant (Fig. 2E). To determine the presence of DTC in long-term survivors, we collected peripheral blood and bone marrow in 3 WTe and 3 cKO littermates that were free from BLI-detectable metastases 175 days after tumor inoculation. We found no significant difference between genotypes in the number of peripheral blood or bone marrow GFP + cells (Fig. 2F, G). Thus, loss of Ncad in Osx + cells does not interfere with presence of DTC in the bone microenvironment. In all, our data suggest that Ncad expression by osteogenic cells does not affect DTC engraftment and retention in the bone.

3.3. Loss of N-cadherin in bone marrow stromal cells does not alter adhesion to tumor cells

We then asked whether loss of Ncad disrupts adhesion between osteogenic stromal cells and cancer cells in vitro. To this end, we applied two approaches, 1) the ability of tumor and stromal cells to form functional gap junctions, which requires cells to adhere and anchor to each other, and 2) cell adhesion mediated-drug resistance. To model heterotypic adhesion between tumor Ecad and bone Ncad, we used bone marrow stromal cells (BMSC), which are enriched in osteogenic cells expressing Ncad [5,7,12] and the gap junction protein connexin43 (Cx43) [33]. As shown earlier, breast cancer 4T1 cells express Ecad but not Ncad mRNA [39] (Sup. Fig. 1A); they also express Cx43 (Sup. Fig. 3A). To test for IGJC, DiI-labeled 4T1 tumor cells were parachuted on a monolayer of calcein-loaded BMSC isolated from either WTe or cKO. As illustrated in Fig. 3A, after 1 h incubation, DiI-stained cells (quadrant ii) that came in contact with calcein-loaded WTe BMSC (iii, blue arrows) were also green (iv), demonstrating diffusion of calcein from donor BMSC to acceptor tumor cells. Parachuting DiI-labeled 4T1 tumor cells onto cKO calcein-loaded BMSC resulted in similar uptake of green fluorescence by acceptor tumor cells (Fig. 3B); thus indicating that lack of Ncad in osteogenic cells does not alter their ability to engage in direct cell–cell interactions. In fact, quantitation of cell coupling using FACS on cells released after 8-h co-incubation demonstrated that almost the entire population of 4T1 tumor cells had taken calcein from donor BMSC, regardless of their genotype (Fig. 3C). The need of cell–cell contact for calcein diffusion was confirmed by lack of calcein uptake by 4T1 tumor cells when seeded on the opposite side of a transwell system with calcein-labeled WTe BMSC (Fig. 3C). Validation experiments also demonstrated that calcein diffusion from tumor cells to BMSC was mediated by Cx43, since *Gja1* knock-down by shRNA in 4T1 cells (Sup. Fig. 3A) greatly reduced calcein transfer to acceptor cells (Sup. Fig. 3B, C). We also tested the melanoma cell line B16-F10, which expresses Ncad [40], in the GJIC assay. Calcein-labeled B16-F10 cells were also able to pass the fluorescent dye to both WTe and cKO BMSC, whereas when tumor and bone marrow cells

Table 1
Subcutaneaus tumor growth in N-cadherin deficient and wild type mice.

Expt. Number	Genotype	N	Final Day Post-injection	Tumor size at excision (mm^3)[a]	P[b]
1[c]	*Cdh2*$^{fl/fl}$ (Wte)	5F, 6 M	10	413.4[e]	0.041
	Cdh2$^{fl/fl}$;Osx-cre (cKO)	4 M		501.2 (291.5)	
2[c]	*Cdh2*$^{fl/fl}$ (Wte)	4F, 3 M	13	838.4 (327.5)	0.008
	Cdh2$^{fl/fl}$;Osx-cre (cKO)	3F, 2 M		1065.1 (271.1)	
3[d]	Ai9;*Cdh*$^{fl/fl}$ (Wte)	2F, 2 M	13	307.3 (66.8)	0.003
	Ai9;*Cdh2*$^{fl/fl}$;Osx-cre (cKO)	2F, 3 M		711 (355.2)	
4[d]	*Cdh2*$^{fl/fl}$ (Wte)	3F, 6 M	15	863.5 (299.1)	0.002
	Cdh2$^{fl/fl}$;Osx-cre (cKO)	2F, 4 M		1229.9 (434.8)	

F females, M males; [a]mean (SD); [b]for genotype effect (two-way ANOVA on repeated measurements during the entire observation period). [c]Doxycycline treatment (during pregnancy and until weaning), [d]no doxycycline treatment. [e]n = 2.

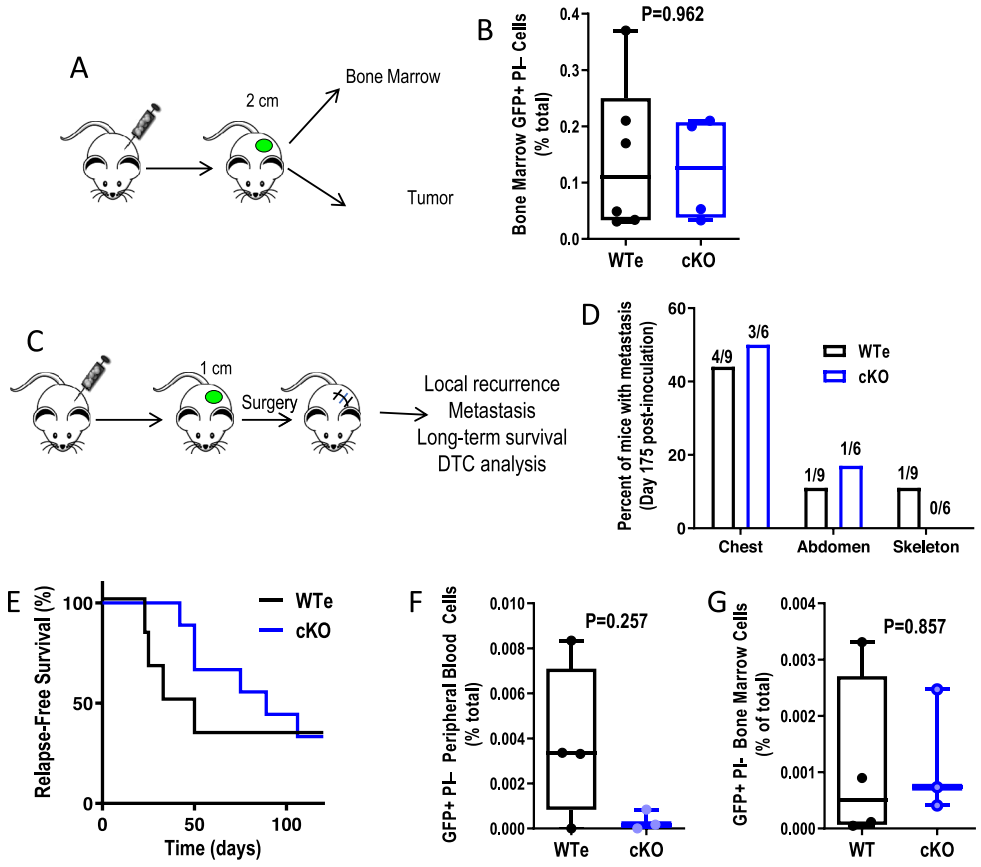

Fig. 2. Metastatic dissemination of extraskeletal tumors. (A) BO1 cells were inoculated into WTe and cKO and let grow until they reached 2 cm maximum diameter, when tumors and bone marrow were harvested for flow cytometry. (B) Percentage of GFP+ cells in the bone marrow of WTe and cKO mice. (C) Mice were inoculated subcutaneously with BO1 cells; when tumors reached 1 cm of maximum diameter, they were surgical resected and mice were followed for recurrence, distress symptoms (dyspnea, severe weight loss), survival and evidence of metastases by BLI. (D) Percent of mice without local recurrence but with metastasis (by BLI) at day 175 post-inoculation at three different sites. (E) Kaplan-Meyer analysis of relapse-free survival following primary MFP tumor resection (subjects at risk: WTe = 9, cKO = 6; p = 0.476, Log-rank test). Percent of GFP+ cells relative to total cells by flow cytometry of (F) peripheral blood, or (G) bone marrow of long-term survivors without evidence of tumor progression (negative for recurrence in multiple BLI) at day 175 from inoculation. P-values shown in B, F, and G calculated using Mann-Whitney test.

were separated in a transwell system, no calcein transfer occurred (not shown). Thus, even though not all BMSC would be expected to be targeted by Osx-Cre, these results show no evidence that ablation of *Cdh2* in Osx expressing cells (which are abundantly present in BMSC cultures) alters the ability of these cells to directly communicate with tumor cells via gap junctions.

To test cell adhesion mediated-drug resistance, we co-cultured 4T1 breast cancer cells with BMSC isolated from either WTe or *Cdh2*-cKO littermates, and treated them with eribulin, a microtubule inhibitor used in breast cancer therapy [30]. As expected for microtubule dysfunction, exposure of 4T1 to eribulin resulted in a 4-fold increase in the number of cells in G2. By contrast, only half as many 4T1 cells co-cultured with either WTe or cKO BMSC were arrested in G2, suggesting that co-culture with the stroma decreased sensitivity to chemotherapy, and that this effect is not altered by lack of Ncad in ostegenic cells (Fig. 3D). In all, these experiments show that Ncad deletion in stromal cells does not prevent osteogenic cell adhesion and communication with tumor cells.

3.4. Ncad is expressed in a subset of Osx + cells present in the tumor microenvironment and at extra-skeletal sites

The larger subcutaneous tumor growth and the apparent increased severity of metastatic disease in cKO mice prompted us to ask whether Ncad deletion in extra-skeletal cells may be involved in modulating tumorigenesis. Indeed, in a parallel study using the Ai9:Osx-cre reporter mouse we found that a proportion of cells in the stromal component of tumors generated by subcutaneous inoculation of breast (BO1) and melanoma (B16-10) cells express red fluorescence (TdT^{Osx}+) [41,42]. We confirmed the presence of TdT^{Osx}+ cells in the stromal component (GFP– CD45– population) of orthotropic BO1 tumors grown in either WTe mice or in *Cdh2* cKO mice, with no significant differences between the two genotypes (Fig. 4A). FACS analysis using an anti-Ncad antibody further revealed that a sub-population (5–6%) of these tumor-associated TdT^{Osx}+ GFP– CD45– cells express Ncad (Fig. 4B). Although in the adult skeleton Osx expression is generally thought to be restricted to bone, emerging data suggest that Osx-Cre also targets extra-skeletal tissues in adult mice [43–45]. Since the lungs are frequent sites of breast cancer metastasis, we isolated lung cells from non-tumor bearing mice by collagenase digestion and identified TdT^{Osx}+ cells by FACS (about 4% of the entire population; Fig. 4Ci, ii). TdT^{Osx}+ were also present, in smaller proportion, in the subcutaneous tissue (Fig. 4Ciii, iv). In cultures of stromal cells isolated from MFP of normal mice, TdT^{Osx}+ cells exhibited a flattened, irregular shape with multiple small processes, remindful of osteoblasts or fibroblasts (Fig. 4Di, ii); and in lung sections, TdT+ cells were scattered in the lung interstitial tissue (Fig. 4Diii, iv). Flow cytometry confirmed expression of Ncad in approximately 5% of the TdT^{Osx}+ population of MFP cells, and in a smaller proportion of lung interstitial cells. In both tissues, Ncad+ cells were undetectable among the TdT^{Osx}+ population in cKO; Ai9 mice (Fig. 4E, F). Thus, Ncad is expressed in subsets of Osx+ cells present in the

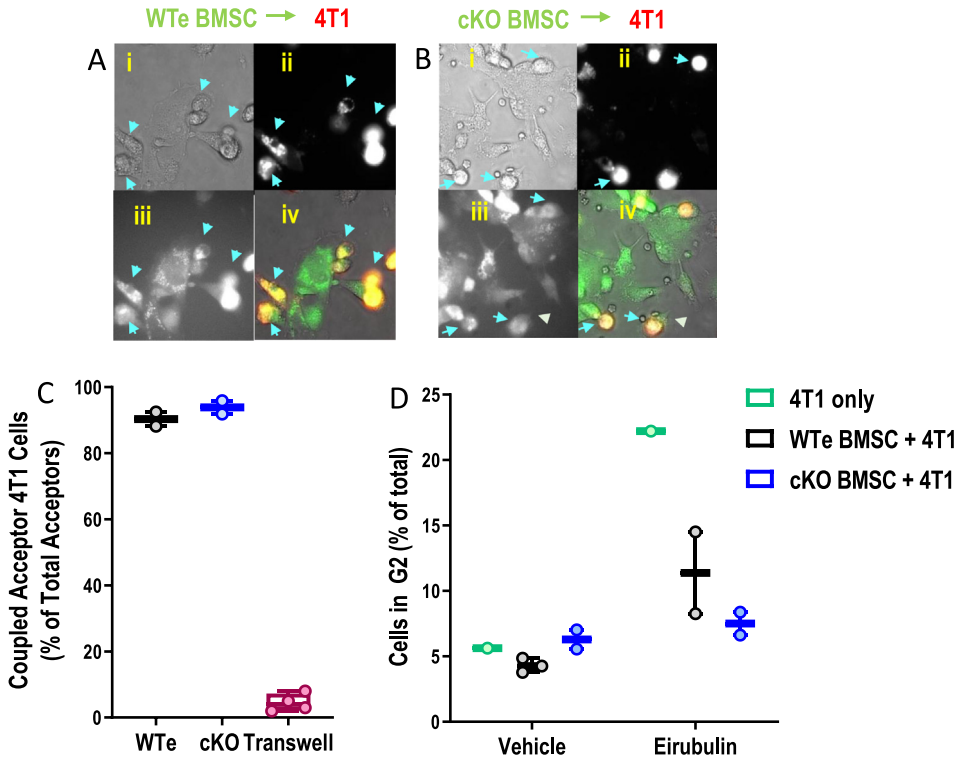

Fig. 3. Intercellular gap junctional communication (IGJC) and cell contact dependent chemoresistance. DiI-labeled 4T1 cells were parachuted on a monolayer of calcein-loaded BMSC isolated from (A) WTe or (B) cKO mice. Live optical imaging showing (i) phase contrast, (ii) DiI fluorescence, (iii) calcein fluorescence, and (iv) merged image. Arrowheads indicate DiI-labeled cells that have taken calcein (in yellow in the merged image) as index of IGJC. Quantitation of IGJC as percentage of (C) DiI + Calcein + 4T1 breast cancer cells relative to all DiI cells assessed by flow cytometry. In the Transwell condition, cells were grown on opposite sides of a semi-permeable membrane to allow fluid exchange but prevent cell–cell contact. (D) 4T1 cells cultured alone or in the presence of WTe or cKO BMSC, as indicated, were exposed to 200 nM eirubulin or vehicle for 24 h and processed for cell cycle assessment by flow cytometry. Data are presented as percentage of cells in G2 relative to the total number of cells. (For interpretation of the references to colour in this figure legend, the reader is referred to the web version of this article.)

tumor microenvironment at extra-skeletal sites, but also in normal lung and subcutanoues tissue.

3.5. Loss of N-cadherin induces protumorigenic gene expression signatures in tumor microenvironment Osx+ cells

To explore how loss of Ncad may affect the transcriptome of tumor microenvironment Osx+ cells, we applied RNAseq analysis to cells isolated from subcutaneous BO1 tumors grown in Ai9;Osx-cre or Ai9;cKO mice. After tumor excision, cell suspensions were sorted after GFP (tumor cells) and CD45 (hematopoietic cells) subtraction into TdT^{Osx}+ and TdT– populations (Sup. Fig. 4), and mRNA extracted for library preparation and high-throughput sequencing. We obtained an average of 32 million reads for each of the cDNA libraries, with an average of 72% reads uniquely mapped to the mouse reference genome. After the gene counts were filtered for ribosomal and low expressing genes, the counts were Voom transformed with Limma. We applied an unbiased method to evaluate the relationship among the four groups of cells (WTe TdT^{Osx}+, Wte TdT–, cKO TdT^{Osx}+, cKO TdT–). Principal components analysis revealed that nearly 90% of the total variance was accounted for in the first principal component, indicating that the cell sorting procedures were adequate, and that most of the changes between conditions observed were biological rather than technical in origin. Further scrutiny revealed that Wte TdT– cells (representing tumor microenvironment stromal cells that are not targeted by Osx-Cre) from *Cdh2* deficient and control mice clustered close to each other, while TdT + cells from tumors grown in Ai9;cKO mice grouped separately with moderate cluster separation between groups. The moderate cluster separation indicated that the differentials at the gene level would be modest in both significance and magnitude and the post-hoc differential expression analysis results with Limma would need to be adjusted accordingly (Fig. 5A). We first analyzed the transcriptional profile of tumor associated TdT^{Osx}+ and TdT^{Osx}– cells from WTe (Ai9) mice and found > 2000 genes differentially regulated (Fig. 5B). Pathway analysis showed that TdT^{Osx}+ upregulate genes involved in collagen production and extracellular matrix processing, relative to TdT^{Osx}– (Fig. 5C). Univariate analysis revealed that TdT^{Osx}+ express significantly higher abundance of osteoblast genes than do TdT^{Osx}– cells, specifically RANKL (*Tnfsf11*), periostin (*Postn*), parathyroid hormone receptor (*Pthr1*), the chondro-osteogenic specific metalloproteinases *Mmp9* and *Mmp13* and fibrillar collagens *Col27a1*, *Col24a1*, and of course, *Col1a1* and *Col1a2* mRNA (Fig. 5C). Interestingly, TdT^{Osx}+ cells express significantly less alkaline phosphatase (*Alpl*) mRNA. On the other hand, analysis of canonical cancer associated fibroblast (CAF) markers revealed that TdT^{Osx}+ express significantly less FSP1 (*S100a4*) and *Cav1* mRNA relative to TdT^{Osx}– cells, with the exception of *Fsp*, which was slightly increased. Other markers shared by CAF and osteolineage cells, such as *Igtb1*, α-SMA (*Acta2*) and *Pdgfa/b* were also marginally higher in TdT^{Osx}+ relative to TdT– cells (Fig. 5D).

Further analysis of differentially expressed genes between cKO TdT^{Osx}+ and WTe TdT+ cells revealed that using $p \leq 0.05$ cut-off, 551 genes were up-regulated in cKO TdT^{Osx}+ cells with $\log_2$ fold-changes between 0.49 and 7.89, while 739 genes were down-regulated with a $\log_2$ fold-change between −0.50 and 7.30. Increasing the stringency to $p \leq 0.01$ and an absolute value $\log_2$ fold-change ≥ 2, we found 33 up-regulated genes and 85 down-regulated genes (Fig. 6A). To further elucidate the functional

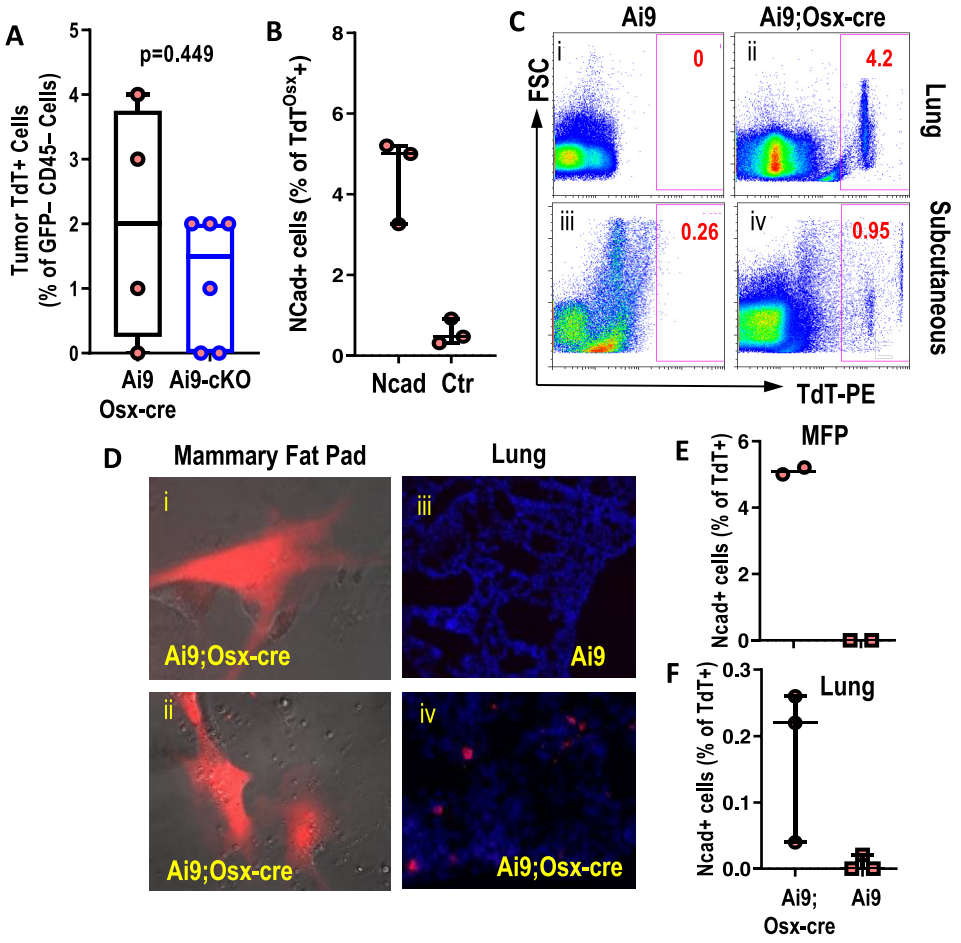

Fig. 4. TdT^{Osx}+ and Ncad+ cells among lung and subcutaneous cells. (A) Percentage of TdT+ cells of total GFP– CD45– cells in the stromal component of orthotropic BO1 tumors grown in either Ai9;Osx-cre or Ai9;cKO mice, assessed by flow cytometry. (B) Percentage of Ncad+ cells among TdT^{Osx}+ GFP– CD45– cells in the stromal component of orthotropic BO1 tumors grown in either Ai9;Osx-cre mice. (C) Flow cytometry analysis of TdT+ cells isolated from (i, ii) lungs and (iii, iv) subcutaneous tissue of Ai9 or Ai9; Osx-cre mice. (D) Cultures of (i, ii) mammary fat pad stromal cells of Ai9;Osx-cre mice showing large, flattened cells with red fluorescence; and frozen sections of lungs of (iii) Ai9 or (iv) Ai9;Osx-cre mice showing a few, scattered TdT+ cells in the lung interstitial tissue. Quantitation of flow cytometry data showing the proportion of Ncad+ cells in (E) the mammary fat pad (MFP) and (F) lung tissue of Ai9; Osx-Cre and Ai9;cKO mice. (For interpretation of the references to colour in this figure legend, the reader is referred to the web version of this article.)

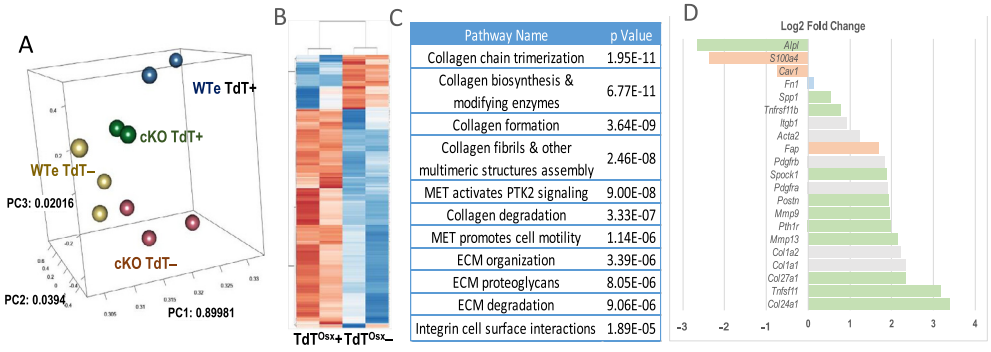

Pathway Name	p Value
Collagen chain trimerization	1.95E-11
Collagen biosynthesis & modifying enzymes	6.77E-11
Collagen formation	3.64E-09
Collagen fibrils & other multimeric structures assembly	2.46E-08
MET activates PTK2 signaling	9.00E-08
Collagen degradation	3.33E-07
MET promotes cell motility	1.14E-06
ECM organization	3.39E-06
ECM proteoglycans	8.05E-06
ECM degradation	9.06E-06
Integrin cell surface interactions	1.89E-05

Fig. 5. RNAseq analysis of tumor associated TdT^{Osx}+ cells. Cells isolated from BO1 tumors grown in Ai9;Osx-cre or Ai9; *Osx-cre* mice were FAC-sorted for TdT+ and TdT– from the GFP– CD45– population (to exclude tumor and hematopoietic cells) for RNAseq analysis. (A) 3-D plot representing principal component analysis, where each dot represents cells from one tumor (one mouse). (B) Heat map and (C) pathway analysis of differentially expressed genes. (D) Univariate analysis of differential expression of molecular markers for osteogenic cells (green), or CAF (orange), or shared markers (gray). (For interpretation of the references to colour in this figure legend, the reader is referred to the web version of this article.)

impact of these differentially expressed genes, we performed a GAGE $\log_2$ fold-change analysis of all tested genes against the Molecular Signature Database (MSigDb). Among the 1,290 genes identified as significantly differentially regulated between cKO TdT^{Osx}+ and WTe TdT + cells, we found 212 genes that contained transcription factor binding motifs across 31 significantly enriched MSigDb transcription factor motif target gene sets with Benjamini-Hochberg adjusted p-values ≤ 0.05 (Sup. Fig. 5). Frequency analysis of the 212 genes across the gene sets revealed that *Nfat*, *Foxo4*, *MAZ*, *Sp1*, *Lef1*, *Meis1*, and *Chx10* had the greatest number of recur-

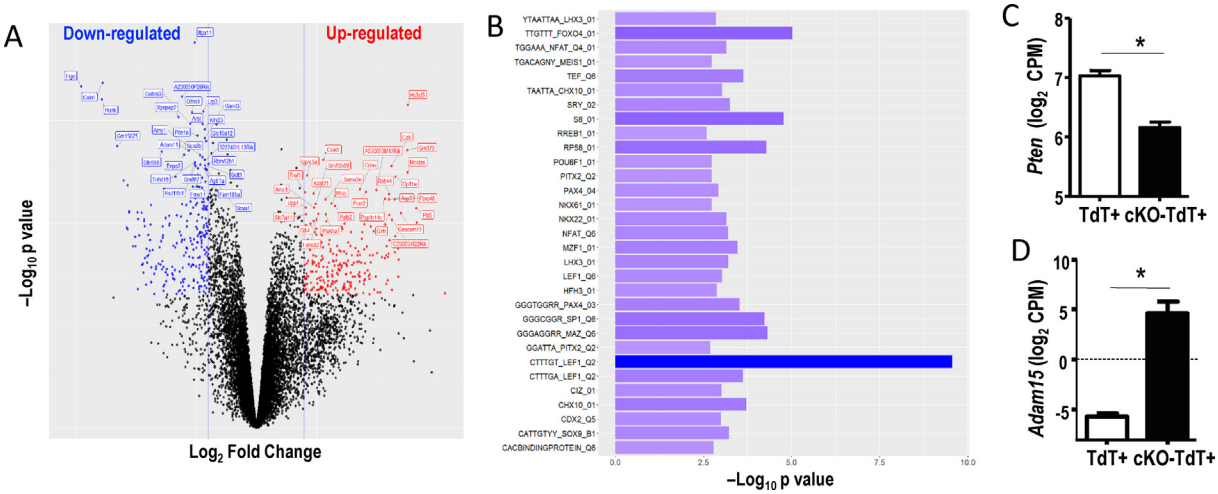

Fig. 6. Transcriptional profile of Ncad+ and Ncad– TdT^{Osx}+ cells. Cells isolated from BO1 tumors grown in Ai9;Osx-cre or Ai9; *Osx-cre* mice were FAC-sorted for TdT+ and TdT– cells after subtraction of GFP+ and CD45+ cells. (A) Volcano plot showing differentially up-regulated (red) and down-regulated (blue) genes in TdT+ cells from tumors grown in cKO relative to those grown in WTe mice. (B) Heat map of transcription factor binding motifs significantly differentially up-regulated (red) or down-regulated (blue) in TdT+ cells from tumors grown in cKO relative to those grown in WTe mice. Univariate analysis of (C) *Pten* and (D) *Adam15* in TdT^{Osx}+ cells from tumors grown in either WTe or KO mice, *P < 0.01, *t*-test for unpaired samples. (For interpretation of the references to colour in this figure legend, the reader is referred to the web version of this article.)

ring genes, with *Lef1* being the most highly represented (Fig. 6B). Univariate analysis also revealed that the tumor suppressor gene, *Pten* was downregulated in cKO TdT^{Osx}+ cells; while the pro-tumorigenic protease *Adam15*, which is negatively regulated by *Pten* [46], was up-regulated in cKO TdT^{Osx}+ relative to WTe TdT+ cells (Fig. 6C, D). By contrast, there was no significant differential expression of other cadherins or cell adhesion molecules in cKO TdT^{Osx}+ cells. Of note, *Cdh11* was the most abundantly expressed, consistent with a stromal, osteolineage nature of these cells (Sup. Fig. 6A, B). Pathway analysis through KEGG pointed towards activation of the Ras/ERK and PI3K pathways in cKO TdT^{Osx}+ cells (Sup. Fig. 7A, B).

4. Discussion

These studies demonstrate that loss of Ncad in osteogenic (Osx-cre-targeted) cells does not alter tumor growth in bone or metastasis to bone but results in an unexpected pro-tumorigenic effect in extra-skeletal tumors. This effect is not related to tumor cells adhesive properties, but rather to an anti-tumorigenic action of Ncad in previously unrecognized Osx+ cells present in the stromal compartment of extra-skeletal tumors; in the absence of Ncad, these cells acquire a pro-tumorigenic transcriptional signature.

Ncad in osteogenic cells has been proposed as a mechanism for the recruitment and retention of DTC in the bone marrow, via heterotypic interactions with Ecad on tumor cells [26]. Of note, mechanically active heterotypic interactions between Ncad in CAF and Ecad in tumor cells facilitate tumor cell migration and tumor growth [47]. Yet, clinical studies using Ncad antagonists have yielded discordant results [24,25]. Since adhesion of DTC to the bone microenvironment can favor the permanence and chemoresistance of cancer cells capable of initiating metastatic relapse, even in the absence of immediate bone metastatic growth [48], we leveraged a model of conditional *Cdh2* deletion in the osteogenic lineage [5,12], to investigate whether Ncad is indeed the molecular anchor tethering cancerous cells to the bone. Contrary to expectations, we found that Ncad in osteogenic cells is not necessary for the growth of tumor cells inoculated into the bone, nor for tumor-induced osteolysis. Notably, loss of Ncad in the osteogenic lineage did not prevent initial tumor cell dissemination (in the presence of a large tumor), long-term permanence of disseminated cells after tumor resection, or late-recurring metastatic growth. Therefore these data, obtained in a validated genetic model of selective *Cdh2* ablation in Osx+ cells [5,12], do not support a prominent role of Ncad in the establishment or development of bone metastases. It should be noted that most cell types express a variety of adhesion molecules, and such redundancy may well explain why lack of Ncad does not alter the ability of BMSC, which contain osteogenic cells, to engage in cell–cell adhesive interactions with tumor cells expressing either Ecad or Ncad. Thus, the anti-tumorigenic action on Ncad is most likely independent of cell–cell adhesion.

The most striking, unexpected findings of this work are the larger growth of tumors and higher frequency of metastasis at extra-skeletal sites in mice with Osx-cre-driven *Cdh2* ablation. As noted, while Osx expression is generally thought to be restricted to bone, emerging data suggest that Osx is also present in extra-skeletal tissues in adult mice [43–45]. Here, we demonstrate that Osx-cre targets small populations of stromal cells within the tumor microenvironment outside of the bone, and in normal subcutaneous and lung tissue. While these observations do not exclude that bone resident Osx-cre-targeted cells contribute to extra-skeletal effects via endocrine mechanisms [49], or mobilization of hematopoietic cells [50], it is likely that these tumor associated TdT^{Osx}+ cells participate in shaping the microenvironment of extra-skeletal tumors. The relatively low frequency of TdT^{Osx}+ cells in healthy subcutaneous tissue (<1%) compared to nearly 15% in subcutaneous tumor tissue suggests that either TdT^{Osx}+ cells are recruited to the tumor, or the tumor cues stromal cell expression of Osx or expansion of the resident TdT^{Osx}+ population. Cells with osteogenic capacity are present in the circulation of animals and humans [51], and recent data suggest that circulating osteocalcin positive cells may represent an early marker of bone metastasis [52]. In related work with other collaborators, we also find Osx+ cells in peripheral blood, but these cells are hematopoietic in origin [41,42], and ontogenetically unrelated to the tumor associated TdT^{Osx}+ cells described here, which were selected for not expressing CD45. In fact, our transcriptomic analysis show that relative to the TdT^{Osx}– population, tumor associated TdT^{Osx}+ cells have a mesenchymal, osteogenic signature, as they up-regulate genes involved in collagen matrix production and processing, as well as osteoblast-specific markers. Of note, markers of CAF not shared with osteoblasts are either down-regulated or modestly

changed in TdT^{Osx}+ cells, suggesting that these cells are a distinct cell population of the tumor microenvironment with pro-osteogenic features, but likely without the capacity of mineralizing, since *Alpl*, necessary for mineralization, is selectively down-regulated. Regardless of their origin and function, these tumor associated TdT^{Osx}+ cells might well be the cells through which Ncad exerts its restraining effect on tumor progression; an effect opposite to its pro-tumorigenic action in CAF [47]. These results indicate that Ncad exerts multiple and even opposite actions on tumorigenesis depending on the cell context where it is expressed, most likely through different regulatory mechanisms; while in CAF Ncad favors tumor spreading via cell–cell adhesion and motility, inhibition of tumor progression is via modulation of specific signaling pathways in TdT^{Osx}+ cells. These diverse, cell-specific actions may explain the inconsistent results of clinical oncology research on Ncad antagonism.

The proportion of Ncad+ cells within the TdT^{Osx}+ population in the tumor microenvironment may seem low but is consistent with the fraction of bone marrow stromal cells that express Ncad in healthy mice (about 10%); and *Cdh2* ablation in Osx+ cells results in low bone mass, growth delay and loss of osteogenic precursors [4,5]. Of note, increased tumor growth in *Cdh2* cKO mice does not reflect loss of cells with an anti-tumorigenic profile, since the number of TdT^{Osx}+ cells is not altered by *Cdh2* ablation. By contrast, transcriptomic analysis of these tumor associated TdT^{Osx}+ cells show that multiple signaling pathways involved in tumor growth are altered by loss of Ncad (Fig. 7). As occurs in cells of bone [5], *Cdh2* ablation up-regulates *Lef1* and its targets in tumor associated TdT^{Osx}+ cells, confirming that even at extra-skeletal sites Ncad restrains Wnt signaling. Furthermore, up-regulation of Ras and ERK signaling components and of pro-tumorigenic targets with consensus sequences for Sp1 and Nfat in TdT^{Osx}+ cells from cKO mice suggest inhibition of the Ras/MAPK cascade by Ncad. Ras hyperactivation is associated with secretion of pro-tumorigenic factors by CAF [53]; and Sp1 and Nfat regulate matrix proteases and other secretory factors associated with cancer invasiveness [54]. Inhibition of Ras/ERK by Ncad has been reported in other cell systems [11,55], consistent with observations that Ncad restrains tumor growth in K-ras-induced murine pancreatic tumors in a cell-autonomous fashion [22,56]. Moreover, consistent with Ncad inhibition of PI3K signaling [11], loss of Ncad in tumor associated TdT^{Osx}+ cells increases PI3K signal components and up-regulates PI3K-dependent pro-tumorigenic targets with consensus sequences for Nfat, MAZ, Sp1 and Lef1. Further, loss of Ncad decreases expression of *Pten*, a PI3K regulator with lipid and phosphatase activity [57] that restrains stromal support of tumorigenesis via extracellular matrix remodeling and inhibition of immune cell infiltration and angiogenesis [58,59]. Consistently, down-regulation of *PTEN*, possibly via AKT hyper-activation, has been reported in melanoma cells after treatment with the Ncad inhibitor, ADH-1 [23]. Downstream of these pathways, we found increased expression of *Adam15*, a member of a family of catalytically active disintegrin membrane metalloproteinases that function as molecular signaling switches, shed membrane bound growth factors, and cleave type I cadherins, such as Ecad and Ncad [60]. Notably, Adam15 activation is associated with increased metastatic potential of cancer [61]. Thus, increased cancer growth in *Cdh2* cKO mice may be contributed to by enhanced Adam15-dependent release of pro-tumorigenic factors in the tumor microenvironment.

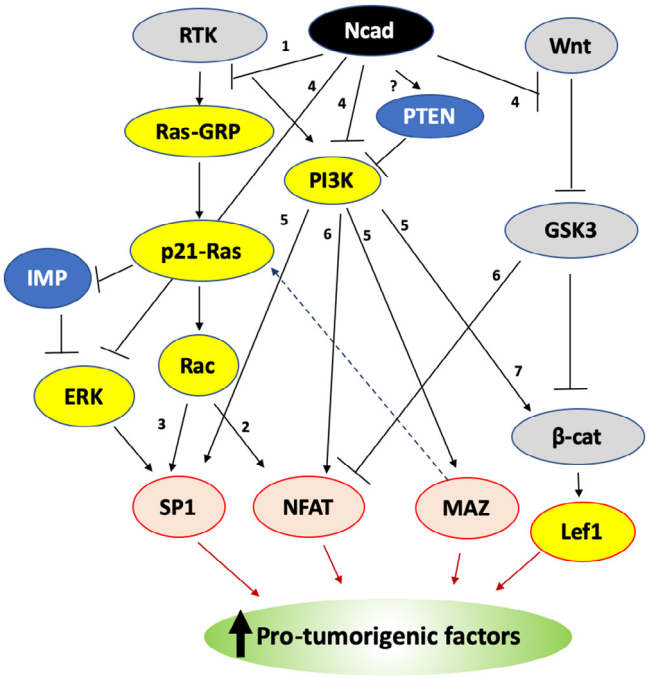

Fig. 7. Working model of Ncad regulation of pro-tumorigenic signaling in tumor associated TdT^{Osx}+ cells. Yellow: up-regulated genes; Blue: down-regulated genes; Grey: annotated upstream signaling events; Red border: transcription factors with up-regulated target genes. (For interpretation of the references to colour in this figure legend, the reader is referred to the web version of this article.)

Overall, our results are consistent with a biologic model whereby loss of Ncad hyperactivates Ras, PI3K and β-catenin signaling converging on activation of Nfat, Sp1, MAZ and Lef1 and increased production of pro-tumorigenic factors (Fig. 7). Our model challenges the dogma that the primary role of Ncad is to promote cancer growth via adhesive interactions between tumor and microenvironment cells and expands its function to modulation of specific signaling pathways active in tumorigenesis. One limitation of these studies is that we used syngeneic murine models of breast cancer that, though widely used, may not fully recapitulate human cancer biology; therefore, it remains possible that Ncad-driven adhesion may be more important in metastatic growth in bone in humans. Furthermore, the transcriptomic findings must be validated and should be considered as hypothesis building rather then definitive mechanisms.

We have discovered a new, unexpected role for Ncad in the interplay between cancer and its microenvironment, recasting Ncad from a simple mediator of cell–cell adhesion to more active player in microenviroment-tumor cell interactions. We have also discovered a previously unrecognized branch of the mesenchymal/osteogenic lineage that contributes to extra-skeletal tumor growth and may serve yet unknown functions outside of the bone. These observations broaden the concept of cellular heterogeneity within the tumor microenvironment and offer a new platform for targeting the stroma with the purpose of inhibiting tumor growth and metastasis.

Contributions

F.F. designed and performed most of the work presented, analyzed the entire dataset, and co-wrote the manuscript; J.X. contributed to most in vivo experiments, and generated the flow cytometry data; X.S. provided supervision with tumor inoculation and contributed to all the work with the tumor cell lines; E.T. performed most of the informatics analysis, and helped with interpretation of these data and manuscript preparation; R.N. contributed to the analysis of tumor osteolysis; G.F. performed RT-qPCR on cadherin expression, G.L. helped with RNA extraction for RNAseq analysis; K.W. contributed to conceiving the project and supervised

most of the experimentation on tumor biology; R.C. contributed to conceiving and designing the entire project, reviewed the entire data set and co-wrote the manuscript. F.F. and R.C. take full responsibility for data integrity and analysis.

CRediT authorship contribution statement

Francesca Fontana: Conceptualization, Methodology, Validation, Formal analysis, Investigation, Data curation, Writing - original draft, Writing - review & editing. **Jingyu Xiang:** Investigation. **Xinming Su:** Supervision. **Eric Tycksen:** Validation, Formal analysis, Data curation, Writing - original draft, Writing - review & editing. **Rachel Nassau:** Investigation. **Gregory Fox:** Investigation. **Giulia Leanza:** Investigation. **Katherine Weilbaecher:** Conceptualization, Methodology, Validation, Formal analysis, Resources, Writing - original draft, Writing - review & editing, Supervision, Funding acquisition. **Roberto Civitelli:** Conceptualization, Methodology, Validation, Formal analysis, Resources, Data curation, Writing - original draft, Writing - review & editing, Supervision, Project administration, Funding acquisition.

Declaration of Competing Interest

The authors declare the following financial interests/personal relationships which may be considered as potential competing interests:

Roberto Civitelli: Mereo Biopharma (research support); Merck & Co., Eli-Lilly, Amgen (stock ownership). All other co-authors have no competing interests.

Acknowledgements

This work was supported by the National Institutes of Health (R01 CA243383 to RC, P01 CA100730, CA154737, CA097250 to KNW), the Barnes-Jewish Hospital Foundation (to RC and KNW), the Siteman Cancer Center Investment Program (to RC and KNW), the Washington University Institute for Clinical and Translational Sciences "Just-In-Time" Program (funded by NIH CTSA Grant UL1 TR002345, to RC and FF), and the St. Louis Men's Group Against Cancer (to KNW). We also thank the Core Center for Musculoskeletal Biology and Medicine (funded by P30 AR057235), and the Genome Technology Access Center (partially supported by P30 CA91842 to the Siteman Cancer Center and by Grant UL1 TR002345 from the National Center for Research Resources, a component of the NIH, and NIH Roadmap for Medical Research). This publication is solely the responsibility of the authors and does not necessarily represent the official view of NCRR or NIH.

Appendix A. Supplementary data

Supplementary data to this article can be found online at https://doi.org/10.1016/j.jbo.2021.100356.

References

[1] K.N. Weilbaecher, T.A. Guise, L.K. McCauley, Cancer to bone: a fatal attraction, Nat. Rev. Cancer 11 (6) (2011) 411–425.
[2] M. Janiszewska, M.C. Primi, T. Izard, Cell adhesion in cancer: Beyond the migration of single cells, J. Biol. Chem. 295 (8) (2020) 2495–2505.
[3] B.M. Gumbiner, Regulation of cadherin-mediated adhesion in morphogenesis, Nat. Rev. Mol. Cell Biol. 6 (8) (2005) 622–634.
[4] A. Di Benedetto, M. Watkins, S. Grimston, V. Salazar, C. Donsante, G. Mbalaviele, G.L. Radice, R. Civitelli, N-cadherin and cadherin 11 modulate postnatal bone growth and osteoblast differentiation by distinct mechanisms, J. Cell Sci. 123 (15) (2010) 2640–2648.
[5] F. Fontana, C.L. Hickman-Brecks, V.S. Salazar, L. Revollo, G. Abou-Ezzi, S.K. Grimston, S.Y. Jeong, M. Watkins, M. Fortunato, Y. Alippe, D.C. Link, G. Mbalaviele, R. Civitelli, N-cadherin regulation of bone growth and homeostasis is osteolineage stage-specific, J. Bone Miner Res. 32 (6) (2017) 1332–1342.
[6] E. Haÿ, F.-X. Dieudonné, Z. Saidak, C. Marty, J. Brun, S. Da Nascimento, P. Sonnet, P.J. Marie, N-cadherin/wnt interaction controls bone marrow mesenchymal cell fate and bone mass during aging, J. Cell Physiol. 229 (11) (2014) 1765–1775.
[7] A.M. Greenbaum, L.D. Revollo, J.R. Woloszynek, R. Civitelli, D.C. Link, N-cadherin in osteolineage cells is not required for maintenance of hematopoietic stem cells, Blood 120 (2) (2012) 295–302.
[8] O. Bromberg, B.J. Frisch, J.M. Weber, R.L. Porter, R. Civitelli, L.M. Calvi, Osteoblastic N-cadherin is not required for microenvironmental support and regulation of hematopoietic stem and progenitor cells, Blood 120 (2) (2012) 303–313.
[9] C.F. Lai, S.-L. Cheng, G. Mbalaviele, C. Donsante, M. Watkins, G.L. Radice, R. Civitelli, Accentuated ovariectomy-induced bone loss and altered osteogenesis in heterozygous N-cadherin null mice, J. Bone Miner. Res. 21 (12) (2006) 1897–1906.
[10] K. Ando, K. Uemura, A. Kuzuya, M. Maesako, M. Asada-Utsugi, M. Kubota, N. Aoyagi, K. Yoshioka, K. Okawa, H. Inoue, J. Kawamata, S. Shimohama, T. Arai, R. Takahashi, A. Kinoshita, N-cadherin regulates p38 MAPK signaling via association with JNK-associated leucine zipper protein: implications for neurodegeneration in Alzheimer disease, J. Biol. Chem. 286 (9) (2011) 7619–7628.
[11] E. Haÿ, A. Nouraud, P.J. Marie, A. Bergmann, N-cadherin negatively regulates osteoblast proliferation and survival by antagonizing Wnt, ERK and PI3K/Akt signalling, PLoS One 4 (12) (2009) e8284, https://doi.org/10.1371/journal.pone.0008284.
[12] L. Revollo, J. Kading, S.Y. Jeong, J. Li, V. Salazar, G. Mbalaviele, R. Civitelli, N-cadherin restrains PTH activation of Lrp6/beta-catenin signaling and osteoanabolic action, J. Bone Miner. Res. 30 (2) (2015) 274–285.
[13] E. Hay, E. Laplantine, V. Geoffroy, M. Frain, T. Kohler, R. Muller, P.J. Marie, N-cadherin interacts with axin and LRP5 to negatively regulate Wnt/beta-catenin signaling, osteoblast function, and bone formation, Mol. Cell Biol. 29 (4) (2009) 953–964.
[14] K.M. Mrozik, O.W. Blaschuk, C.M. Cheong, A.C.W. Zannettino, K. Vandyke, N-cadherin in cancer metastasis, its emerging role in haematological malignancies and potential as a therapeutic target in cancer, BMC Cancer 18 (1) (2018) 939.
[15] X. Qian, A. Anzovino, S. Kim, K. Suyama, J. Yao, J. Hulit, G. Agiostratidou, N. Chandiramani, H.M. McDaid, C. Nagi, H.W. Cohen, G.R. Phillips, L. Norton, R.B. Hazan, N-cadherin/FGFR promotes metastasis through epithelial-to-mesenchymal transition and stem/progenitor cell-like properties, Oncogene 33 (26) (2014) 3411–3421.
[16] E. Scarpa, A. Szabó, A. Bibonne, E. Theveneau, M. Parsons, R. Mayor, Cadherin Switch during EMT in Neural Crest Cells Leads to Contact Inhibition of Locomotion via Repolarization of Forces, Dev. Cell 34 (4) (2015) 421–434.
[17] M.J. Wheelock, Y. Shintani, M. Maeda, Y. Fukumoto, K.R. Johnson, Cadherin switching, J. Cell Sci. 121 (Pt 6) (2008) 727–735.
[18] G. Li, K. Satyamoorthy, M. Herlyn, N-cadherin-mediated intercellular interactions promote survival and migration of melanoma cells, Cancer Res. 61 (9) (2001) 3819–3825.
[19] H. Tanaka, E. Kono, C.P. Tran, H. Miyazaki, J. Yamashiro, T. Shimomura, L. Fazli, R. Wada, J. Huang, R.L. Vessella, J. An, S. Horvath, M. Gleave, M.B. Rettig, Z.A. Wainberg, R.E. Reiter, Monoclonal antibody targeting of N-cadherin inhibits prostate cancer growth, metastasis and castration resistance, Nat. Med. 16 (12) (2010) 1414–1420.
[20] Y. Shintani, Y. Fukumoto, N. Chaika, P.M. Grandgenett, M.A. Hollingsworth, M.J. Wheelock, K.R. Johnson, ADH-1 suppresses N-cadherin-dependent pancreatic cancer progression, Int. J. Cancer 122 (1) (2008) 71–77.
[21] C.K. Augustine, Y. Yoshimoto, M. Gupta, P.A. Zipfel, M.A. Selim, P. Febbo, A.M. Pendergast, W.P. Peters, D.S. Tyler, Targeting N-cadherin enhances antitumor activity of cytotoxic therapies in melanoma treatment, Cancer Res. 68 (10) (2008) 3777–3784.
[22] Y. Su, J. Li, C. Shi, R.H. Hruban, G.L. Radice, N-cadherin functions as a growth suppressor in a model of K-ras-induced PanIN, Oncogene 35 (25) (2016) 3335–3341.
[23] R.S. Turley, Y. Tokuhisa, H. Toshimitsu, M.E. Lidsky, J.C. Padussis, A. Fontanella, W. Deng, C.K. Augustine, G.M. Beasley, M.A. Davies, M.W. Dewhirst, D.S. Tyler, Targeting N-cadherin increases vascular permeability and differentially activates AKT in melanoma, Ann. Surg. 261 (2) (2015) 368–377.
[24] N. Yarom, D. Stewart, R. Malik, J. Wells, L. Avruch, D. J. Jonker, Phase I clinical trial of Exherin (ADH-1) in patients with advanced solid tumors, Curr. Clin. Pharmacol. 8 (1) (2013) 81–88.
[25] G.M. Beasley, J.C. Riboh, C.K. Augustine, J.S. Zager, S.N. Hochwald, S.R. Grobmyer, B. Peterson, R. Royal, M.I. Ross, D.S. Tyler, Prospective multicenter phase II trial of systemic ADH-1 in combination with melphalan via isolated limb infusion in patients with advanced extremity melanoma, J. Clin. Oncol. 29 (9) (2011) 1210–1215.
[26] H. Wang, C. Yu, X. Gao, T. Welte, A. Muscarella, L. Tian, H. Zhao, Z. Zhao, S. Du, J. Tao, B. Lee, T. Westbrook, S.C. Wong, X. Jin, J. Rosen, C.K. Osborne, X.-F. Zhang, The osteogenic niche promotes early-stage bone colonization of disseminated breast cancer cells, Cancer Cell 27 (2) (2015) 193–210.
[27] N. Percie du Sert, V. Hurst, A. Ahluwalia, S. Alam, M.T. Avey, M. Baker, W.J. Browne, A. Clark, I.C. Cuthill, U. Dirnagl, M. Emerson, P. Garner, S.T. Holgate, D. W. Howells, N.A. Karp, S.E. Lazic, K. Lidster, C.J. MacCallum, M. Macleod, E.J. Pearl, O.H. Petersen, F. Rawle, P. Reynolds, K. Rooney, E.S. Sena, S.D. Silberberg, T. Steckler, H. Würbel, I. Boutron, The ARRIVE guidelines 2.0: Updated

guidelines for reporting animal research, PLoS Biol. 18 (7) (2020) e3000410, https://doi.org/10.1371/journal.pbio.3000410.
[28] S.J. Rodda, A.P. McMahon, Distinct roles for Hedgehog and canonical Wnt signaling in specification, differentiation and maintenance of osteoblast progenitors, Development 133 (16) (2006) 3231–3244.
[29] X. Su, D.H. Floyd, A. Hughes, J. Xiang, J.G. Schneider, O. Uluckan, E. Heller, H. Deng, W. Zou, C.S. Craft, K. Wu, A.C. Hirbe, D. Grabowska, M.C. Eagleton, S. Townsley, L. Collins, D. Piwnica-Worms, T.H. Steinberg, D.V. Novack, P.B. Conley, M.A. Hurchla, M. Rogers, K.N. Weilbaecher, The ADP receptor P2RY12 regulates osteoclast function and pathologic bone remodeling, J. Clin. Invest. 122 (10) (2012) 3579–3592.
[30] J. Xiang, M.A. Hurchla, F. Fontana, X. Su, S.R. Amend, A.K. Esser, G.J. Douglas, C. Mudalagiriyappa, K.E. Luker, T. Pluard, F.O. Ademuyiwa, B. Romagnoli, G. Tuffin, E. Chevalier, G.D. Luker, M. Bauer, J. Zimmermann, R.L. Aft, K. Dembowsky, K.N. Weilbaecher, CXCR4 protein epitope mimetic antagonist POL5551 disrupts metastasis and enhances chemotherapy effect in triple-negative breast cancer, Mol. Cancer Ther. 14 (11) (2015) 2473–2485.
[31] X. Su, A.K. Esser, S.R. Amend, J. Xiang, Y. Xu, M.H. Ross, G.C. Fox, T. Kobayashi, V. Steri, K. Roomp, F. Fontana, M.A. Hurchla, B.L. Knolhoff, M.A. Meyer, E.A. Morgan, J.C. Tomasson, J.S. Novack, W. Zou, R. Faccio, D.V. Novack, S.D. Robinson, S.L. Teitelbaum, D.G. DeNardo, J.G. Schneider, K.N. Weilbaecher, Antagonizing integrin beta3 increases immunosuppression in cancer, Cancer Res. 76 (12) (2016) 3484–3495.
[32] M.A. Meyer, J.M. Baer, B.L. Knolhoff, T.M. Nywening, R.Z. Panni, X. Su, K.N. Weilbaecher, W.G. Hawkins, C. Ma, R.C. Fields, D.C. Linehan, G.A. Challen, R. Faccio, R.L. Aft, D.G. DeNardo, Breast and pancreatic cancer interrupt IRF8-dependent dendritic cell development to overcome immune surveillance, Nat. Commun. 9 (1) (2018) 1250.
[33] M. Watkins, S.K. Grimston, J.Y. Norris, B. Guillotin, A. Shaw, E. Beniash, R. Civitelli, R.K. Assoian, Osteoblast connexin43 modulates skeletal architecture by regulating both arms of bone remodeling, Mol. Biol. Cell 22 (8) (2011) 1240–1251.
[34] M. Ogawa, S. Nishikawa, K. Ikuta, F. Yamamura, M. Naito, K. Takahashi, S. Nishikawa, B cell ontogeny in murine embryo studied by a culture system with the monolayer of a stromal cell clone, ST2: B cell progenitor develops first in the embryonal body rather than in the yolk sac, EMBO J. 7 (5) (1988) 1337–1343.
[35] S.J. Bakewell, P. Nestor, S. Prasad, M.H. Tomasson, N. Dowland, M. Mehrotra, R. Scarborough, J. Kanter, K. Abe, D. Phillips, K.N. Weilbaecher, Platelet and osteoclast beta3 integrins are critical for bone metastasis, Proc. Natl. Acad. Sci. USA 100 (24) (2003) 14205–14210.
[36] Ö. Uluçkan, M.C. Eagleton, D.H. Floyd, E.A. Morgan, A.C. Hirbe, M. Kramer, N. Dowland, J.L. Prior, D. Piwnica-Worms, S.S. Jeong, R. Chen, K. Weilbaecher, APT102, a novel adpase, cooperates with aspirin to disrupt bone metastasis in mice, J. Cell Biochem. 104 (4) (2008) 1311–1323.
[37] J.P. Stains, R. Civitelli, A functional assay to assess connexin 43-mediated cell-to-cell communication of second messengers in cultured bone cells, Methods Mol. Biol. 1437 (2016) 193–201.
[38] M.J. Towle, K.A. Salvato, J. Budrow, B.F. Wels, G. Kuznetsov, K.K. Aalfs, S. Welsh, W. Zheng, B.M. Seletsky, M.H. Palme, G.J. Habgood, L.A. Singer, L.V. Dipietro, Y. Wang, J.J. Chen, D.A. Quincy, A. Davis, K. Yoshimatsu, Y. Kishi, M.J. Yu, B.A. Littlefield, In vitro and in vivo anticancer activities of synthetic macrocyclic ketone analogues of halichondrin B, Cancer Res. 61 (3) (2001) 1013–1021.
[39] Y. Elisha, V. Kalchenko, Y. Kuznetsov, B. Geiger, Dual role of E-cadherin in the regulation of invasive collective migration of mammary carcinoma cells, Sci. Rep. 8 (1) (2018) 4986.
[40] M. Hindié, M. Vayssade, M. Dufresne, S. Quéant, R. Warocquier-Clérout, G. Legeay, P. Vigneron, V. Olivier, J.-L. Duval, M.-D. Nagel, Interactions of B16F10 melanoma cells aggregated on a cellulose substrate, J. Cell Biochem. 99 (1) (2006) 96–104.
[41] F. Fontana, B. Ricci, J. Xiang, X. Su, G. Leanza, R. Faccio, K. Weilbaecher, R. Civitelli, N-cadherin in Extra-Skeletal Osterix (Osx) positive cells modulates tumor growth independently of cell-cell adhesion, J Bone Miner Res. 32 (S1) (2017).
[42] B. Ricci, E. Tycksen, H. Celik, J.I. Belle, F. Fontana, R. Civitelli, R. Faccio, Osterix-Cre marks distinct subsets of CD45- and CD45+ stromal populations in extra-skeletal tumors with pro-tumorigenic characteristics, Elife 9 (2020) e54659.
[43] J. Chen, Y.u. Shi, J. Regan, K. Karuppaiah, D.M. Ornitz, F. Long, M. Tjwa, Osx-Cre targets multiple cell types besides osteoblast lineage in postnatal mice, PLoS One 9 (1) (2014) e85161, https://doi.org/10.1371/journal.pone.0085161.
[44] S. Strecker, Y.u. Fu, Y. Liu, P. Maye, Generation and characterization of Osterix-Cherry reporter mice, Genesis 51 (4) (2013) 246–258.
[45] Y. Miura, S. Ota, M. Peterlin, G. McDevitt, S. Kanazawa, A subpopulation of synovial fibroblasts leads to osteochondrogenesis in a mouse model of chronic inflammatory rheumatoid arthritis, JBMR Plus 3 (6) (2019) e10132, https://doi.org/10.1002/jbm4.v3.610.1002/jbm4.10132.
[46] C. Burdelski, M. Fitzner, C. Hube-Magg, M. Kluth, A. Heumann, R. Simon, T. Krech, T. Clauditz, F. Büscheck, S. Steurer, C. Wittmer, A. Hinsch, A.M. Luebke, F. Jacobsen, S. Minner, M.C. Tsourlakis, B. Beyer, T. Steuber, I. Thederan, G. Sauter, J. Izbicki, T. Schlomm, W. Wilczak, Overexpression of the A disintegrin and metalloproteinase ADAM15 is linked to a small but highly aggressive subset of prostate cancers, Neoplasia 19 (4) (2017) 279–287.
[47] A. Labernadie, T. Kato, A. Brugues, X. Serra-Picamal, S. Derzsi, E. Arwert, A. Weston, V. Gonzalez-Tarrago, A. Elosegui-Artola, L. Albertazzi, J. Alcaraz, P. Roca-Cusachs, E. Sahai, X. Trepat, A mechanically active heterotypic E-cadherin/N-cadherin adhesion enables fibroblasts to drive cancer cell invasion, Nat. Cell Biol. 19 (3) (2017) 224–237.
[48] R. Aft, M. Naughton, K. Trinkaus, M. Watson, L. Ylagan, M. Chavez-MacGregor, J. Zhai, S. Kuo, W. Shannon, K. Diemer, V. Herrmann, J. Dietz, A. Ali, M. Ellis, P. Weiss, T. Eberlein, C. Ma, P.M. Fracasso, I. Zoberi, M. Taylor, W. Gillanders, T. Pluard, J. Mortimer, K. Weilbaecher, Effect of zoledronic acid on disseminated tumour cells in women with locally advanced breast cancer: an open label, randomised, phase 2 trial, Lancet Oncol. 11 (5) (2010) 421–428.
[49] C.-S. Devignes, Y. Aslan, A. Brenot, A. Devillers, K. Schepers, S. Fabre, J. Chou, A.-J. Casbon, Z. Werb, S. Provot, HIF signaling in osteoblast-lineage cells promotes systemic breast cancer growth and metastasis in mice, Proc. Natl. Acad. Sci. USA 115 (5) (2018) E992–E1001.
[50] C. Engblom, C. Pfirschke, R. Zilionis, J. Da Silva Martins, S.A. Bos, G. Courties, S. Rickelt, N. Severe, N. Baryawno, J. Faget, V. Savova, D. Zemmour, J. Kline, M. Siwicki, C. Garris, F. Pucci, H.-W. Liao, Y.-J. Lin, A. Newton, O.K. Yaghi, Y. Iwamoto, B. Tricot, G.R. Wojtkiewicz, M. Nahrendorf, V. Cortez-Retamozo, E. Meylan, R.O. Hynes, M. Demay, A. Klein, M.A. Bredella, D.T. Scadden, R. Weissleder, M.J. Pittet, Osteoblasts remotely supply lung tumors with cancer-promoting SiglecF(high) neutrophils, Science 358 (6367) (2017) eaal5081, https://doi.org/10.1126/science:aal5081.
[51] J. Feehan, K. Nurgali, V. Apostolopoulos, A. Al Saedi, G. Duque, Circulating osteogenic precursor cells: building bone from blood, EBioMedicine 39 (2019) 603–611.
[52] K.-H. Lee, K.J. Lee, T.-Y. Kim, F. Hutomo, H.J. Sun, G.J. Cheon, S.I. Park, S.W. Cho, S.-A. Im, Circulating osteocalcin-positive cells as a novel diagnostic biomarker for bone metastasis in breast cancer patients, J Bone Miner Res 35 (10) (2020) 1838–1849.
[53] J.-P. Coppé, C.K. Patil, F. Rodier, Y.u. Sun, D.P. Muñoz, J. Goldstein, P.S. Nelson, P.-Y. Desprez, J. Campisi, J. Downward, Senescence-associated secretory phenotypes reveal cell-nonautonomous functions of oncogenic RAS and the p53 tumor suppressor, PLoS Biol. 6 (12) (2008) e301, https://doi.org/10.1371/journal.pbio.0060301.
[54] J. Shou, J. Jing, J. Xie, L. You, Z. Jing, J. Yao, W. Han, H. Pan, Nuclear factor of activated T cells in cancer development and treatment, Cancer Lett. 361 (2) (2015) 174–184.
[55] H. Turner, M. Gomez, E. McKenzie, A. Kirchem, A. Lennard, D.A. Cantrell, Rac-1 regulates nuclear factor of activated T cells (NFAT) C1 nuclear translocation in response to Fcepsilon receptor type 1 stimulation of mast cells, J. Exp. Med. 188 (3) (1998) 527–537.
[56] X. Wang, A.A. Thant, K. Machida, Y. Hiraiwa, H. Iwata, S. Matsuda, M. Hamaguchi, Suppression of cell growth by ectopic expression of N-cadherin, Int. J. Clin. Oncol. 12 (5) (1998) 1097–1101.
[57] M.P. Myers, I. Pass, I.H. Batty, J. Van der Kaay, J.P. Stolarov, B.A. Hemmings, M. H. Wigler, C.P. Downes, N.K. Tonks, The lipid phosphatase activity of PTEN is critical for its tumor supressor function, Proc. Natl. Acad. Sci. USA 95 (23) (1998) 13513–13518.
[58] A. Bronisz, J. Godlewski, J.A. Wallace, A.S. Merchant, M.O. Nowicki, H. Mathsyaraja, R. Srinivasan, A.J. Trimboli, C.K. Martin, F. Li, L. Yu, S.A. Fernandez, T. Pécot, T.J. Rosol, S. Cory, M. Hallett, M. Park, M.G. Piper, C.B. Marsh, L.D. Yee, R.E. Jimenez, G. Nuovo, S.E. Lawler, E.A. Chiocca, G. Leone, M.C. Ostrowski, Reprogramming of the tumour microenvironment by stromal PTEN-regulated miR-320, Nat. Cell Biol. 14 (2) (2012) 159–167.
[59] A.J. Trimboli, C.Z. Cantemir-Stone, F.u. Li, J.A. Wallace, A. Merchant, N. Creasap, J.C. Thompson, E. Caserta, H. Wang, J.-L. Chong, S. Naidu, G. Wei, S.M. Sharma, J. A. Stephens, S.A. Fernandez, M.N. Gurcan, M.B. Weinstein, S.H. Barsky, L. Yee, T. J. Rosol, P.C. Stromberg, M.L. Robinson, F. Pepin, M. Hallett, M. Park, M.C. Ostrowski, G. Leone, Pten in stromal fibroblasts suppresses mammary epithelial tumours, Nature 461 (7267) (2009) 1084–1091.
[60] M.J. Duffy, E. McKiernan, N. O'Donovan, P.M. McGowan, Role of ADAMs in cancer formation and progression, Clin. Cancer Res. 15 (4) (2009) 1140–1144.
[61] G. Lorenzatti Hiles, A. Bucheit, J.R. Rubin, A. Hayward, A.L. Cates, K.C. Day, L. El-Sawy, L.P. Kunju, S. Daignault, C.T. Lee, M. Liebert, M. Hussain, M.L. Day, N. Kyprianou, ADAM15 is functionally associated with the metastatic progression of human bladder cancer, PLoS One 11 (3) (2016) e0150138, https://doi.org/10.1371/journal.pone.0150138.